

Single-cycle terahertz pulses with amplitudes exceeding 1 MV/cm generated by optical rectification in LiNbO₃

H. Hirori,^{1,2,a)} A. Doi,^{2,3} F. Blanchard,^{1,2} and K. Tanaka^{1,2,4}

¹Institute for Integrated Cell-Material Sciences, Kyoto University, Sakyo-ku, Kyoto 606-8501, Japan

²CREST, Japan Science and Technology Agency, Kawaguchi, Saitama 332-0012, Japan

³Olympus Corporation, Hachioji-shi, Tokyo 192-8512, Japan

⁴Department of Physics, Graduate School of Science, Kyoto University, Sakyo-ku, Kyoto 606-8502, Japan

(Received 26 January 2011; accepted 8 February 2011; published online 2 March 2011)

Using the tilted-pump-pulse-front scheme, we generate single-cycle terahertz (THz) pulses by optical rectification of femtosecond laser pulses in LiNbO₃. In our THz generation setup, the condition that the image of the grating coincides with the tilted-optical-pulse front is fulfilled to obtain optimal THz beam characteristics and pump-to-THz conversion efficiency. By using an uncooled microbolometer-array THz camera, it is found that the THz beam leaving the output face of the LN crystal can be regarded as a collimated rather than point source. The designed focusing geometry enables tight focus of the collimated THz beam with a spot size close to the diffraction limit, and the maximum THz electric field of 1.2 MV/cm is obtained. © 2011 American Institute of Physics. [doi:10.1063/1.3560062]

Recent successful developments in efficient high-power terahertz (THz) pulse generation has created many promising applications such as in large-scale object imaging, medical diagnosis and treatment, and remote sensing techniques for security issues.^{1,2} In addition, intense THz pulses allow for study of unexplored nonlinear phenomena such as coherent THz manipulation of quantum states,^{3,4} high-order harmonic generation,⁵ nonlinear optical processes, and nonlinear transport phenomena in solids.⁶⁻¹²

Since Hebling *et al.*¹³ (2002) proposed a tilted-pump-pulse-front scheme for efficient phase-matched THz pulse generation using LiNbO₃ crystals, the technique has been rapidly developing. This technique has demonstrated the possibility of THz pulse generation with energies on the scale of 10 μ J by using an amplified Ti:sapphire laser with low repetition frequencies.^{14,15} To make the technique versatile for applications and useful for study of unexplored nonlinear phenomena, a generation setup to obtain optimal THz beam characteristics and a maximized THz peak field is required. A recent detailed analysis of the scheme predicted that the imaging errors in the setup consisting of a grating and lenses can lead to distortion in THz intensity profile after the LiNbO₃ output surface.¹⁶ This distortion could create strong and ambiguous divergence in the THz beam, causing inaccuracy in optimal optics design for THz measurement, thereby limiting its applications.

In this paper, we report the generation of single-cycle THz pulses using the tilted-pump-pulse-front scheme with a 1.3 mol % MgO-doped stoichiometric LiNbO₃ (LN) crystal. In the THz generation setup, the condition that the image of the grating coincides with the tilted-optical-pulse front is fulfilled to obtain optimal THz beam characteristics and pump-to-THz conversion efficiency. The propagation characteristics of the THz beam leaving the output face of the LN crystal were measured by an uncooled microbolometer-array THz camera. The results show that the THz beam had divergence of 52 ± 5 mrad in the horizontal direction for 1 THz.

The designed focusing geometry for the collimated THz beam enables tight focus onto the electro-optic (EO) crystal with a spot size of around 300 μ m for 1 THz, and a peak THz electric field of 1.2 MV/cm and energy conversion efficiency of $\sim 1 \times 10^{-3}$ are obtained.

Figures 1(a) and 1(b) show schematics of the THz pulse

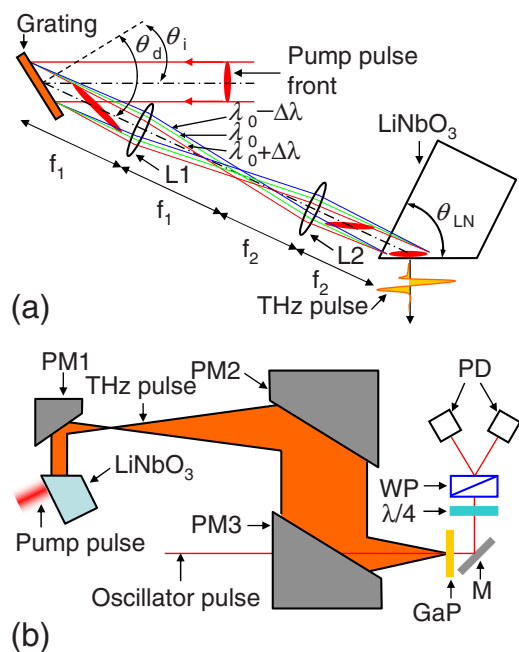


FIG. 1. (Color online) (a) Schematic of the THz pulse generation setup for the tilted-pump-pulse-front scheme. The 4f-lens configuration consists of two cylindrical lenses L1 and L2 with respective focal lengths of 250 and 150 mm in horizontal direction. The grating we used has a groove density of 1800 cm^{-1} . The incident angle θ_i and diffracted angle θ_d of the grating are set at 35.3° and 55.7°, respectively. The LN prism angle θ_{LN} is 62°. A half-wave plate (not shown) between L1 and L2 changes a polarization of pump pulse from horizontally to vertically direction. (b) Schematic of the EO sampling setup. The off-axis parabolic mirrors PM1, PM2, and PM3 have effective focal lengths of 10, 100, and 50 mm, respectively. Their respective diameters are 10, 50, and 50 mm. M: mirror, WP: Wollaston prism, PD: photodetector.

^{a)}Electronic mail: hirori@icems.kyoto-u.ac.jp.

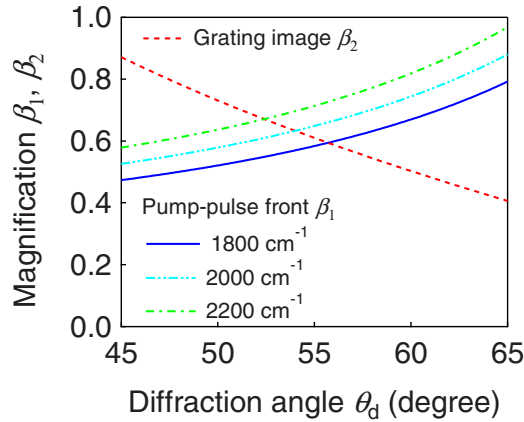


FIG. 2. (Color online) Calculated magnifications of the pump-pulse front β_1 for the different grating grooves and the grating image β_2 as a function of θ_d in Eqs. (1) and (2), respectively.

generation setup using the tilted-pump-pulse-front scheme and the EO sampling setup, respectively. For a pump source, we used an amplified Ti:sapphire laser that provided a pulse energy of 4 mJ, a full width at half-maximum (FWHM) intensity of 85 fs, a central wavelength of 780 nm, and a repetition rate of 1 kHz. The optical pulses from the oscillator with a repetition rate of 80 MHz synchronized with the amplified pulses were used for the EO sampling.

To match the noncollinear velocity of the pump v_p^{gr} and THz pulses v_{THz} in the LN crystal for efficient THz generation, i.e., $v_p^{gr} \cos \gamma = v_{THz}$, we tilted the pump-pulse front angle γ by using the grating and two cylindrical lenses, as shown in Fig. 1(a). The angle γ is described as below:¹⁶

$$\tan \gamma = \frac{m\lambda_0 p}{n_p^{gr} \beta_1 \cos \theta_d}, \quad (1)$$

where m , θ_d , and p are the diffraction order, diffraction angle, and groove density of a grating, respectively. λ_0 and n_p^{gr} are the central pump pulse wavelength and group refractive index of the LN crystal at the pump pulse wavelength, respectively, and β_1 is the horizontal magnification factor of the lenses for the pump-pulse front. The LN crystal angle θ_{LN} in Fig. 1(a) should be the same as the γ for the THz pulse coming out perpendicularly to the LN output face.

To obtain optimal THz beam characteristics and pump-to-THz conversion efficiency, the tilt angle θ of the grating image inside the LN should coincide with that of the pump-pulse front γ because the temporal pump-pulse duration across the image of the grating is approximately minimal. The tilt angle θ is described as follows:¹⁶

$$\tan \theta = n\beta_2 \tan \theta_d, \quad (2)$$

where n is the refractive index of the LN crystal for the pump pulse and β_2 is the horizontal magnification factor of the lenses for the grating image.

Figure 2 shows the calculated curves of the horizontal magnification factors β_1 for the different grating grooves and β_2 as functions of θ_d .¹⁷ When the magnification factors have a same value, the condition of matching the angles is fulfilled. For efficient generation of around 1 THz, we have set θ and $\gamma = 62^\circ$ in Eqs. (1) and (2).¹⁸ As shown in Fig. 2, the curve β_1 for the grating groove of 1800 cm^{-1} (solid line) and β_2 (dashed line) have the same value of 0.59 when $\theta_d = 55.7^\circ$. In the actual setup, the horizontal magnification fac-

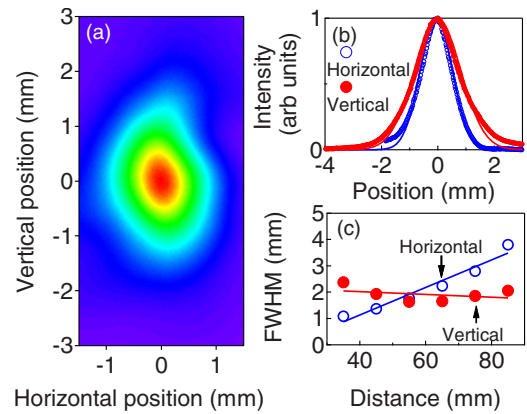


FIG. 3. (Color online) (a) THz intensity image and (b) its cross-section profiles with Gaussian fits measured at 45 mm from the LN output surface. (c) Measured spot size is a function of propagation distance. Solid lines show linear fits.

tor of $f_2/f_1 = \beta_1 = \beta_2 = 0.6$, which is close to the calculated ideal value of 0.59, is realized by using $4f$ -lens geometry as shown in Fig. 1(a).

Figures 3(a) and 3(b) show the THz intensity image and cross-section profiles at 45 mm from the LN output surface, respectively. The THz intensity image passing through a 300 GHz width band-pass filter for 1 THz (Murata Manufacturing Co., Ltd., MMBPF40-1000), can be measured by a 320×240 pixel uncooled microbolometer THz camera with $23.5 \mu\text{m}$ pixel pitch from NEC Corporation (model IRV-T0830). In Fig. 3(b), the solid lines show the corresponding Gaussian fits, and diameters at FWHM in vertical and horizontal directions are 1.9 mm and 1.3 mm, respectively. The image is vertically elongated because the incident pump pulse with a spot diameter of 5.2 mm at FWHM was horizontally magnified with a factor of 0.6 and there are residual imaging errors and THz absorptions in LN.

Figure 3(c) shows the spot size as a function of propagation distance. The THz beam has a divergence of $54 \pm 5 \text{ mrad}$ and $-5 \pm 5 \text{ mrad}$ in horizontal and vertical directions, respectively. The fairly collimated beam with radially symmetric Gaussian beams shown in Figs. 3(b) and 3(c) indicates that the THz generation optics with $4f$ -lens geometry can make the angle of the grating image coincide with that of the pump-pulse front. Otherwise, the spatially asymmetric intensity profile and strong divergence of THz beam could be induced.¹⁶

To obtain the maximized peak THz field, the generated collimated THz beam confirmed by the THz camera measurement should be expanded, collimated, and focused tightly. As shown in Fig. 1(b), we developed the focusing geometry onto the EO crystal by three off-axis parabolic mirrors PM1, PM2, and PM3, assuming the collimated THz beam source rather than the point source.

Figures 4(a) and 4(b) show the THz temporal profile, measured by THz EO sampling with a $300 \mu\text{m}$ thick GaP detection crystal, and its Fourier components, respectively. In the EO detection, six high-resistivity Si attenuators were inserted to reduce the field amplitude before the GaP detection crystal.¹⁹ The maximum modulation of the balanced photo-detector signals I_A and I_B measured at the peak THz field, i.e., $(I_A - I_B)/(I_A + I_B)$, is 0.44 with the Si attenuators; this value corresponds to the electric field of 1.2 MV/cm without the Si attenuators.²⁰ The spectrum in Fig. 4(b) has a maxi-

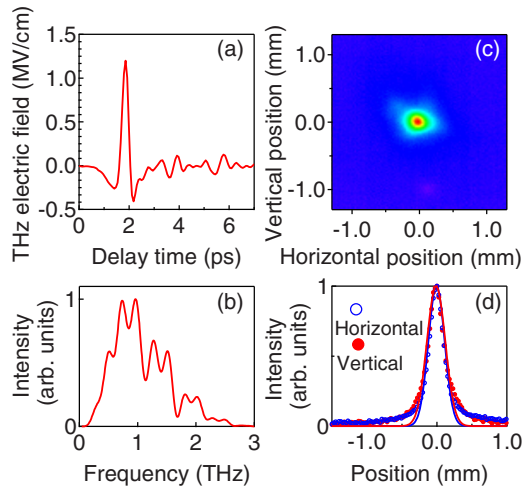


FIG. 4. (Color online) (a) Measured THz temporal profile and (b) its Fourier components. (c) The THz image measured at the focused point after the last off-axis parabolic mirror [PM3 in Fig. 1(b)]. (d) Cross-section intensity profiles of the THz image in (c) with Gaussian fits.

imum intensity around 1 THz and absorption lines caused by water vapor because dry air purging was not performed.

Figures 4(c) and 4(d) show the THz image and intensity profiles, respectively, at the focused point after the last off-axis parabolic mirror [PM3 in Fig. 1(b)]. The intensity profiles in Fig. 4(d) show that the both THz spot diameters at FWHM in vertical and horizontal directions were around 300 μm . The small spot size close to the diffraction limit implies that our designed focusing optics shown in Fig. 1(b) directs a sufficiently tightly focused THz beam. The total pulse energy was estimated to $\sim 2 \mu\text{J}$ by integrating the THz intensity both temporally and spatially,²¹ and the energy conversion efficiency was $\sim 1 \times 10^{-3}$. THz pulse energy obtained by a pyroelectric detector (MicroTech Instruments) indicates a larger value of $\sim 3 \mu\text{J}$.

In conclusion, we generated single-cycle THz pulses using the tilted-pump-pulse-front scheme with LN crystals. The careful control of the pump-pulse front improved the beam characteristics of THz pulses with an optimal pump-to-THz conversion efficiency. The spatial shape and divergence of the THz beam leaving the output face of the LN crystal was characterized by the THz camera, and it is found that the THz beam can be regarded as a collimated rather than point source. The designed focusing geometry, assuming generation of the collimated THz beam source, enabled us to tightly focus the THz beam with a spot size of $\sim 300 \mu\text{m}$ for 1 THz, and the peak THz electric field of 1.2 MV/cm with

energy conversion efficiency of $\sim 1 \times 10^{-3}$ were obtained.

We are grateful to Mitsuru Namiki for valuable discussions and also to Iwao Hosako and Kazuhiko Oda for letting us use the THz camera. This study was supported by a Grant-in-Aid for Scientific Research from JSPS (Grant No. 21760038) and from MEXT of Japan (Grant Nos. 18GS0208 and 20104007).

¹M. Tonouchi, *Nat. Photonics* **1**, 97 (2007).

²A. Doi, F. Blanchard, H. Hirori, and K. Tanaka, *Opt. Express* **18**, 18419 (2010).

³B. E. Cole, J. B. Williams, B. T. King, M. S. Sherwin, and C. R. Stanley, *Nature (London)* **410**, 60 (2001).

⁴S. Leinß, T. Kampfrath, K. v. Volkmann, M. Wolf, J. T. Steiner, M. Kira, S. W. Koch, A. Leitenstorfer, and R. Huber, *Phys. Rev. Lett.* **101**, 246401 (2008).

⁵K. Ishikawa, *Phys. Rev. B* **82**, 201402(R) (2010).

⁶L. Razzari, F. H. Su, G. Sharma, F. Blanchard, A. Ayesheshim, H.-C. Bandulet, R. Morandotti, J.-C. Kieffer, T. Ozaki, M. Reid, and F. A. Hegmann, *Phys. Rev. B* **79**, 193204 (2009).

⁷M. C. Hoffmann, J. Hebling, H. Y. Hwang, K.-L. Yeh, and K. A. Nelson, *Phys. Rev. B* **79**, 161201(R) (2009).

⁸H. Hirori, M. Nagai and K. Tanaka, *Phys. Rev. B* **81**, 081305(R) (2010).

⁹K. Shinokita, H. Hirori, M. Nagai, N. Satoh, Y. Kadoya, and K. Tanaka, *Appl. Phys. Lett.* **97**, 211902 (2010).

¹⁰M. Jewariya, M. Nagai, and K. Tanaka, *Phys. Rev. Lett.* **105**, 203003 (2010).

¹¹S. Watanabe, N. Minami, and R. Shimano, *Opt. Express* **19**, 1528 (2011).

¹²W. Kuehn, P. Gaal, K. Reimann, M. Woerner, T. Elsaesser, and R. Hey, *Phys. Rev. Lett.* **104**, 146602 (2010).

¹³J. Hebling, G. Almási, I. Z. Kozma, and J. Kuhl, *Opt. Express* **10**, 1161 (2002).

¹⁴K.-L. Yeh, M. C. Hoffmann, J. Hebling, and K. A. Nelson, *Appl. Phys. Lett.* **90**, 171121 (2007).

¹⁵A. G. Stepanov, L. Bonacina, S. V. Chekalin, and J.-P. Wolf, *Opt. Lett.* **33**, 2497 (2008).

¹⁶J. A. Fülöp, L. Pálfalvi, G. Almási, and J. Hebling, *Opt. Express* **18**, 12311 (2010).

¹⁷Note that m of 1, λ_0 of 780 nm, n_p^{gr} of 2.23, and n of 5.16 are used for the calculation in Fig. 2 (Ref. 18).

¹⁸J. Hebling, A. G. Stepanov, G. Almási, B. Bartal, and J. Kuhl, *Appl. Phys. B: Lasers Opt.* **78**, 593 (2004).

¹⁹M. Jewariya, M. Nagai, and K. Tanaka, *J. Opt. Soc. Am. B* **26**, A101 (2009).

²⁰An EO signal $\Delta I/I$ measured by balanced photodetectors was calibrated to electric field amplitude E_{THz} with the formula $\sin^{-1}(\Delta I/I) = 2\pi n_0^3 r_{41} t_{\text{GaP}}^6 E_{\text{THz}} L / \lambda_0$ [see Q. Wu and X.-C. Zhang, *Appl. Phys. Lett.* **71**, 1285 (1997)]; for the GaP detection crystal used here, the refractive index $n_0 = 3.2$ [see *Handbook of Optical Constants of Solids*, edited by E. D. Palik (Academic, London, 1985)]; the EO coefficient $r_{41} = 0.88 \text{ pm/V}$ [see Y. Berozashvili, S. Machavariani, A. Natsvlishvili, and A. Chirakadze, *J. Phys. D: Appl. Phys.* **22**, 682 (1989)]; the thickness $L = 300 \mu\text{m}$. Fresnel transmission coefficients $t_{\text{GaP}} = 0.46$ for the GaP crystal surface and $t_{\text{Si}} = 0.7$ for the Si wafer were used.

²¹M. Reid and R. Fedosejevs, *Appl. Opt.* **44**, 149 (2005).